Modeling thermal dynamics of active layer soils and near-surface permafrost using a fully coupled water and heat transport model

Yueyang Jiang,[1] Qianlai Zhuang,[2] and Jonathan A. O'Donnell[3]

[1]   Thawing and freezing processes are key components in permafrost dynamics, and these processes play an important role in regulating the hydrological and carbon cycles in the northern high latitudes. In the present study, we apply a well-developed soil thermal model that fully couples heat and water transport, to simulate the thawing and freezing processes at daily time steps across multiple sites that vary with vegetation cover, disturbance history, and climate. The model performance was evaluated by comparing modeled and measured soil temperatures at different depths. We use the model to explore the influence of climate, fire disturbance, and topography (north- and south-facing slopes) on soil thermal dynamics. Modeled soil temperatures agree well with measured values for both boreal forest and tundra ecosystems at the site level. Combustion of organic-soil horizons during wildfire alters the surface energy balance and increases the downward heat flux through the soil profile, resulting in the warming and thawing of near-surface permafrost. A projection of 21st century permafrost dynamics indicates that as the climate warms, active layer thickness will likely increase to more than 3 meters in the boreal forest site and deeper than one meter in the tundra site. Results from this coupled heat-water modeling approach represent faster thaw rates than previously simulated in other studies. We conclude that the discussed soil thermal model is able to well simulate the permafrost dynamics and could be used as a tool to analyze the influence of climate change and wildfire disturbance on permafrost thawing.

1.   Introduction

[2]   Permafrost dynamics in the northern high latitudes are of great interest to the scientific community given the large spatial extent of permafrost [*Lawrence et al.*, 2008], the recent warming in the region [*Arctic Climate Impact Assessment (ACIA)*, 2005; *Serreze et al.*, 2000], and the large amounts of soil organic carbon stored in perennially frozen ground [*Tarnocai et al.*, 2009]. Previous studies have shown that permafrost is influenced directly by climate through changes in air temperature [*Osterkamp*, 2007; *Romanovsky et al.*, 2010] and snow [*Stieglitz et al.*, 2003], or indirectly through disturbance (e.g., wildfire [*Yoshikawa et al.*, 2003]) or local changes in hydrology [*Osterkamp et al.*, 2000; *Jorgenson and Osterkamp*, 2005] which modify the soil thermal regime [*Tchebakova et al.*, 2009; *Jorgenson et al.*, 2010]. Changes in permafrost could in turn contribute to a potential rapid, non-linear response in treeline migration and alterations in the current mosaic structure of boreal forests, as opposed to the previously predicted slow, linear response [*Soja et al.*, 2007]. Field observations and process model studies also indicate that permafrost thaw will result in the release of C from soils to the atmosphere [*Schuur et al.*, 2009], which will serve as a positive feedback to the climate system [*Koven et al.*, 2011; *Schaefer et al.*, 2011; *Schneider von Deimling et al.*, 2012].

[3]   Recent warming in the northern high latitudes [*ACIA*, 2005; *Serreze et al.*, 2000] has initiated permafrost degradation in Alaska [*Osterkamp*, 2007; *Jorgenson et al.*, 2001, 2006], Canada [*Payette et al.*, 2004; *Camill*, 2005], and Russia [*Pavlov*, 1994]. Using a range of future climate scenarios, several modeling studies have projected widespread permafrost degradation across the circumpolar region over the 21st century [*Sazonova et al.*, 2004; *Euskirchen et al.*, 2006; *Lawrence et al.*, 2008, 2012]. However, limitations exist in these permafrost models (e.g., coarse vertical resolution of the soil column, not accounting for non-conductive heat transfer, not fully coupling soil thermal and vertical soil moisture regimes). Furthermore, the effect of fire disturbance on soil thermal and moisture regimes is not incorporated. In

[1]Department of Earth and Atmospheric Sciences, Purdue University, West Lafayette, Indiana, USA.
[2]Department of Earth and Atmospheric Sciences and Department of Agronomy, Purdue University, West Lafayette, Indiana, USA.
[3]United States Geological Survey, Boulder, Colorado, USA.

Corresponding author: Y. Jiang, Department of Earth and Atmospheric Sciences, Purdue University, West Lafayette, IN 47907, USA. (jiang5@purdue.edu)

Table 1. Study Site Information, Measurement Period, and Instrumentation Metadata

Site	Dominant Vegetation	Period	Depth of Soil Temperature Probes (cm)	Depth of Soil Moisture Probes (cm)
Atqasuk	moist acidic tundra	2001–2008	5, 10, 15, 20, 25, 30, 35, 45, 70, 95, 120	15, 25, 40, 50
Betty Pingo	moist and wet nonacidic tundra	2006–2008	5, 10, 15, 20, 25, 30, 40, 50, 60, 70, 80, 95, 120	10, 25, 40
West Dock high	wet nonacidic tundra	2004–2008	5, 10, 15, 20, 25, 30, 35, 45, 70, 95, 120	None
Toolik	moist acidic tundra	1999–2008	8.7, 16, 23.6, 31.2, 38.7, 46.3, 61.6, 76.8, 97.8	9, 12, 38, 39, 68
Sagwon	moist acidic tundra	2006–2008	5, 10, 15, 20, 25, 30, 40, 50, 60, 70, 80, 95, 120	10, 25, 40
Bonanza Creek site 1 (BNZ-W)	white spruce	2003–2008	5, 10, 20, 50, 100, 200	5, 10, 20, 50
Bonanza Creek site 2 (BNZ-B)	black spruce	2003–2008	5, 10, 20, 50, 100, 200	5, 10, 20, 50
Hess Creek (1967)	black spruce	Sep. 2007 – Sep. 2009	3, 6, 11, 20, 74	18
Hess Creek (2003)	black spruce	Sep. 2007 – Sep. 2009	3, 8, 13, 81	6, 10, 18
Hess Creek (HCCN)	black spruce	Sep. 2007 – Sep. 2009	2, 5, 16, 51, 200	3, 7, 22
Hess Creek (HCCS)	black spruce	Sep. 2007 – Sep. 2009	3, 9, 24, 60, 200	None

the boreal region, wildfire disturbance plays an important role in governing the soil thermal dynamics, with several studies documenting post-fire increases in active layer depth (i.e., maximum annual thaw depth in areas underlain by permafrost [*Yoshikawa et al.*, 2003; *Harden et al.*, 2006; *O'Donnell et al.*, 2009]). Through the combustion of surface organic-soil horizons, wildfire can instantaneously change the surface energy balance [*Amiro et al.*, 2006; *Randerson et al.*, 2006] and also modify soil thermal properties for decades following the fire [*O'Donnell et al.*, 2011a]. However, to date, very few process-based ecosystem models take into account wildfire disturbance in the simulation of soil temperature or active layer changes [e.g., *Yi et al.*, 2009]. Therefore, it is necessary to investigate the effect of wildfire disturbance on soil thermal properties and the consequent difference between burned and unburned sites.

[4] So far, large uncertainties exist regarding the influence of warming climate on permafrost ecosystems, given the complex interaction of local factors (e.g., snow, vegetation, soil properties, and soil drainage) that mediate the effects of air temperature on permafrost temperatures. Therefore, continued investigation into the relationship between climate and permafrost dynamics is necessary. A commonly used method for investigating this relationship is to model the heat transport and water movement for the permafrost region using numerical solutions. However, there are several limitations of these previously applied models. For example, the water and heat transfer are not fully coupled in many previous soil thermal models [e.g., *Goodrich*, 1982]. In recent years, land surface permafrost models have been improved following the inclusion of organic soil horizons [*Lawrence and Slater*, 2008], deeper soil layers [*Alexeev et al.*, 2007], and with the inclusion of more accurate boundary and initial conditions [*Lawrence et al.*, 2008]. The incorporation of a dynamic organic soil module in the Terrestrial Ecosystem Model (TEM) by *Yi et al.* [2009] further improves hydrologic and carbon dynamics for black spruce ecosystems.

[5] A model which intimately couples water and heat transport is a suitable tool for the simulation of permafrost dynamics [*Marchenko et al.*, 2008; *Wisser et al.*, 2011]. In this study, we apply a well-developed numerical model [*Hansson et al.*, 2004; *Saito et al.*, 2006] which fully couples heat and water transport to simulate the soil temperature profiles. As demonstrated in *Hansson et al.* [2004], the approach enables numerically stable, energy- and mass-conservative solutions, even with a rapidly changing upper boundary condition and very nonlinear water content and pressure head distributions in the soil profile. It should be noted that lateral water transport was not modeled since convective heat fluxes from lateral flow are small in the studied sites.

[6] In this study, simulations are conducted to model the soil temperature profile from the surface to about 3 m depth for arctic tundra and boreal forest sites in Alaska that differ with respect to vegetation, climate, and disturbance history. The model performance is evaluated by comparing the modeled soil temperature profiles with in situ measurements for boreal forest stands in the discontinuous permafrost zone and for tundra sites in the continuous permafrost zone in Alaska. To examine the effect of fire disturbance on soil thermal properties, we analyze and compare the modeled and measured soil temperatures at burned stands to unburned stands in Hess Creek in interior Alaska [*O'Donnell et al.*, 2011b]. Furthermore, the effects of topography on soil temperatures are tested using soil climate data sets at a north- and a south-facing slope at Hess Creek. In addition, the sensitivity of soil temperature to air temperature at different depths is examined based on ensemble simulations with different upper boundary conditions. Finally, we project the change of active layer thickness (ALT) at multiple sites through the current century (2010–2100) using four IPCC HadCM3 climate change scenarios (A1FI, A2, B1, B2 [*Intergovernmental Panel on Climate Change* (*IPCC*), 2007]). Increases in ALT can exert strong controls on the ecosystem carbon balance [*Goulden et al.*, 1998]. In this study, ALT is determined by the 0°C isotherm, the depth to which liquid water exists continuously from the surface down, as demonstrated in *Wania et al.* [2009].

[7] The overall aim of this study is to evaluate the performance of a recently developed soil thermal algorithm in simulating soil temperatures at multiple sites with different vegetation cover and disturbance history in Alaska's continuous and discontinuous permafrost region. Furthermore, we assess the sensitivity of soil thermal dynamics to projected changes in air temperature. Finally, we explore the effect of the interaction of climate and wildfire disturbance on permafrost dynamics.

2. Data Description

[8] In this study, we use soil temperature and moisture data from 11 sites (Table 1) in arctic and subarctic Alaska to

calibrate and evaluate the model performance. The description of vegetation and soil properties for each site is briefly presented below.

[9] Two data sets from Alaska's boreal region (one white spruce and one black spruce stand) are obtained from the Bonanza Creek Long-term Ecological Research (BNZ-LTER) Data Catalog (http://www.lter.uaf.edu/). The white spruce stand (BNZ-W) is dominated by a dense tall shrub layer, and the forest floor is comprised of a thick mat of feathermoss (*Pleurozium schreberi, Hylocomium splendens*). The black spruce stand (BNZ-B) is dominated by a dense low shrub layer and a thick moss layer [*Werdin-Pfisterer et al.*, 2009]. BNZ-W is not underlain by permafrost while BNZ-B is underlain by discontinuous permafrost. The forest floor thickness ranges from 6 to 20 cm in BNZ-W and 18–30 cm in BNZ-B [*Werdin-Pfisterer et al.*, 2009]. The detailed soil horizon descriptions and classification can be found in C. L. Ping and A. K. Johnson (Soil horizon descriptions/classification and lab analysis, 2000, http://www.lter.uaf.edu/data_detail.cfm?datafile_pkey=149&show=info).

[10] Nine data sets containing soil temperature profiles and soil moisture measurements from five long-term soil-climate stations (Atqasuk, Betty Pingo, West Dock high, Toolik, Sagwon) in Alaska are obtained from the United States Department of Agriculture's National Resources Conservation Service (NRCS, http://www.nrcs.usda.gov). All five profiles are located within arctic tundra ecosystems. It should be noted that there are two separate data sets from two probes for Betty Pingo and four for the West Dock high site. We use each set of data separately. These data sets contain soil temperature monitored at various depths to a maximum of 120 cm and soil water content at several depths with different lengths of observation (Table 1). Measurements are recorded hourly and the detailed site and soil descriptions can be found in *Hinkel and Nelson* [2003].

[11] We also use soil temperature and moisture data collected across a fire chronosequence near Hess Creek in interior Alaska. Measurements are collected from north- and south-facing mature stands (HCCN and HCCS, respectively), a 2003 burned stand (HC03), and a 1967 burn stand (HC67). Sites have been described in detail by *O'Donnell et al.* [2011a]. Briefly, all sites are somewhat poorly drained, and are generally representative of black spruce ecosystems in the discontinuous permafrost zone of Alaska [*Kane et al.*, 2005] and Canada [*Harden et al.*, 1997]. Organic horizon thickness (OHT) varies across the fire chronosequence, averaging 24 ± 1 cm ($\pm$SE) in unburned mature stands, 16 ± 1 cm in the 1967 burn stand, and 14 ± 1 cm in the 2003 burn stand (measured in 2007 [*O'Donnell et al.*, 2011a]). ALT also varies across the fire chronosequences, averaging 45 ± 1 cm in unburned mature stands, 53 ± 2 cm in the 1967 burn stand, and 65 ± 2 cm in the 2003 burn stand (measured in 2007 [*O'Donnell et al.*, 2011b]). Parent material across the chronosequence is composed primarily of ice-rich loess silt deposited during the Late Pleistocene (i.e., yedoma). Volumetric ice content of permafrost at Hess Creek is high, ranging from 60 to 90%. Furthermore, massive ice wedges at some locations account for up to 30–50% of permafrost soil volume. Temperature and moisture data have also been used previously to calibrate

the Geophysical Institute Permafrost Laboratory Model (GIPL) [*O'Donnell et al.*, 2011b].

3. Methods

3.1. Modeling Permafrost Dynamics

[12] We apply the algorithm demonstrated in *Hansson et al.* [2004] to simulate soil temperatures at different depths. In the algorithm, the variably saturated water flow for above- and subzero temperature is described using the modified Richards equation as follows [e.g., *Fayer*, 2000; *Noborio et al.*, 1996]:

$$\frac{\partial \theta_u(h)}{\partial t} + \frac{\rho_i}{\rho_w}\frac{\partial \theta_i(T)}{\partial t} = \frac{\partial}{\partial z}\left[K_{Lh}(h)\frac{\partial h}{\partial z} + K_{Lh}(h) + K_{LT}(h)\frac{\partial T}{\partial z} \right.$$
$$\left. + K_{vh}(\theta)\frac{\partial h}{\partial z} + K_{vT}(\theta)\frac{\partial T}{\partial z} \right] - S \quad (1)$$

where h is the pressure head (m), T is the absolute temperature (K), θ_u is the volumetric unfrozen water content (%), θ is the volumetric liquid water content (%), θ_v ($=\theta_u - \theta$) is the volumetric vapor content expressed as an equivalent water content (%), θ_i is the volumetric ice content (%), t is time (s), z is depth (m), ρ_i is the density of ice (kg m^{-3}), and ρ_w is the density of liquid water (kg m^{-3}). K_{Lh} (m s^{-1}) and K_{LT} (m^2 K^{-1} s^{-1}) are the isothermal and thermal hydraulic conductivities for liquid-phase fluxes due to gradients in h and T, respectively. K_{vh} (m s^{-1}) and K_{vT} (m^2 K^{-1} s^{-1}) are the isothermal and thermal vapor hydraulic conductivities, respectively, and S is a sink term accounting for root water uptake (s^{-1}). Calculations all four conductivities in equation (1) are presented in *Saito et al.* [2006].

[13] The heat transport is governed by the following equation:

$$\frac{\partial C_p T}{\partial t} - L_f \rho_i \frac{\partial \theta_i}{\partial t} + L_0(T)\frac{\partial \theta_v(T)}{\partial t} = \frac{\partial}{\partial z}\left[\lambda(\theta)\frac{\partial T}{\partial z} \right] - C_w \frac{\partial q_l T}{\partial z}$$
$$- C_v \frac{\partial q_v T}{\partial z} - L_0(T)\frac{\partial q_v}{\partial z} - C_w S T \quad (2)$$

where λ is the apparent thermal conductivity of soil (Jm^{-1} s^{-1} K^{-1}) which is a function of moisture content, and q_L and q_v are the flux densities of liquid water and water vapor (m s^{-1}), respectively. C_p (J m^{-3} K^{-1}) is the volumetric heat capacity of the soil, and C_w, C_v (J m^{-3} K^{-1}) are the volumetric heat capacities of the liquid and vapor phases, respectively. L_0 is the volumetric latent heat of vaporization of liquid water (J m^{-3}), and L_f is the latent heat of freezing (approximately 3.34×10^5 J kg^{-1}). Calculations or estimations of all variables in equation (2) are demonstrated in *Hansson et al.* [2004].

[14] Equations (1) and (2) are solved numerically using a finite difference method for both spatial and temporal discretization. As in *Hansson et al.* [2004], Picard iteration is used to linearize both the water flow and heat transport equations.

[15] To account for the effect of snow dynamics on heat and water transport in the long term simulations, here we apply the snow model developed by *Tang and Zhuang* [2010] to simulate the daily snow depth, snow density, as
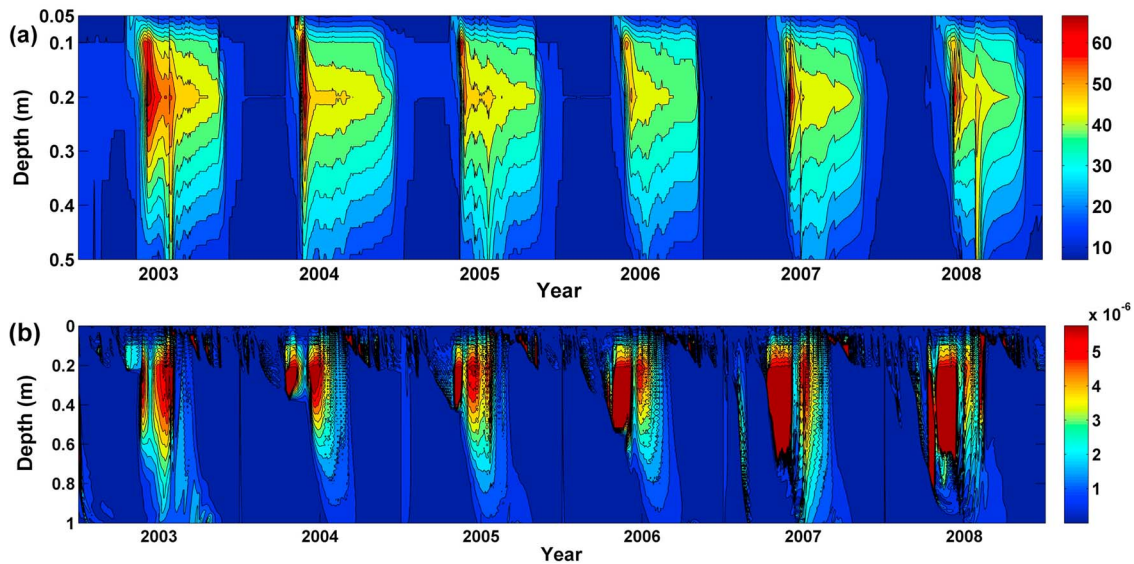
Figure 1. (a) Measured soil water content (%) and (b) calculated thermal hydraulic conductivity ($\mathrm{m^2\,K^{-1}\,s^{-1}}$) at the Bonanza Creek black spruce site from 2003 to 2008.

well as infiltration during spring snowmelt. The upper boundary condition for the modified Richard's equation (equation (1)) to simulate the soil water content is determined by surface infiltration and evapotranspiration [*Zhuang et al.*, 2004]. We use snow climate data (e.g., snow depth) from SNOTEL sites in Alaska (http://ftp.wcc.nrcs.usda.gov/snotel/Alaska/alaska.html), Hess Creek [*O'Donnell et al.*, 2011a] and the Bonanza Creek Long-Term Ecological Research program (http://www.lter.uaf.edu/) to calibrate the snow model. Similar to previous studies [e.g., *Zhuang et al.*, 2001, 2002, 2003, 2004], the snow cover basically functions as a low-conductivity layer in winter, which directly governs the upper boundary condition for the thermal properties of the topsoil layer.

[16] Previous studies [e.g., *Alexeev et al.*, 2007; *Fan et al.*, 2011] have emphasized that the depth of lower boundary in long-term simulations should be deep enough to reasonably simulate the propagations of seasonal, annual, and decadal temperature signals. Here, we set the lower boundary at 50 m deep. Based on soil properties, we classify the top 3.5 m soil profile into six layers with different thickness. The depth step is changed from 1 cm within the top layer to 5 cm within the sixth layer. The soil below 3.5 m until 50 m is classified as the seventh layer and depth step is set as 0.5 m.

[17] The initial condition for the top 3.5 m is generated through linear interpolation for the observed soil temperature profile and soil water content at different depths. Within the seventh layer, the initial soil temperature is assumed to increase by 0.02°C / m and the soil water content is assumed to be constant. For sites having soil moisture measurements (e.g., black spruce site in Bonanza Creek, Figure 1a), we use the measured soil water content instead of the simulated soil moisture content to calculate the soil conductivities within the top six soil layers. Below 3.5 m, the soil moisture is proposed to be constant. Using the equations in *Saito et al.* [2006], we calculate the isothermal (K_{Lh} and K_{vh}) and thermal (K_{LT} and K_{vT}) conductivity at each depth step for each layer. For instance, Figure 1b exhibits the simulated thermal

hydraulic conductivity for the black spruce site at the Bonanza Creek from 2003 to 2008. The measured surface temperature is set as the upper boundary conditions. As in *Fan et al.* [2011], we set the lower boundary condition as a time-dependent heat flux condition by

$$J = \lambda(\theta)\frac{\partial T}{\partial z} \tag{3}$$

where J is the heat flux density ($\mathrm{J\,m^{-1}\,s^{-1}}$).

[18] Our application of this numerical model [*Hansson et al.*, 2004; *Saito et al.*, 2006] has several distinct advantages over other soil thermal models. First, this model can provide a numerically stable solution for the heat and water transport equations even under rapidly changing upper boundary conditions (i.e., surface temperature fluctuations [*Hansson et al.* 2004]). Second, our model uses a numerically stable mass- and energy-conservative algorithm to deal with phase changes, as demonstrated in *Hansson et al.* [2004]. Third, the heat and water transport processes are fully coupled, whereas the moisture-temperature coupling in many models (e.g., Goodrich model) is not physically restricted and synchronous.

3.2. Model Parameterization

[19] To calibrate the model parameters, we first produce 20,000 sets of parameter values using a Latin Hypercube sampler algorithm [*Iman and Helton*, 1988]. In each set, there are totally 17 parameters and each one has a distinct value compared with that from another set. The upper and lower boundary for value range of each parameter is determined by v ± 0.9v, where v is the default value derived from *Hansson et al.* [2004], *Saito et al.* [2006] and *Fayer* [2000]. Second, we conduct 10,000 Monte Carlo simulations using each unique set of parameters. Finally, we determine the parameter values which minimize the root mean square error (RMSE) between modeled daily soil temperatures and the measurement.

Table 2. Parameters Used in the Model Developed by *Hansson et al.* [2004] and *Saito et al.* [2006]

Parameter	Unit	Description
K_S	m s^{-1}	saturated hydraulic conductivity
θ_r	%	residual water contents
θ_S	%	saturated water content
G_{wT}	Unitless	Gradient gain factor
m	Unitless	Empirical parameter
n	Unitless	Empirical parameter
l	Unitless	Empirical parameter
α	m^{-1}	Empirical parameter
Ω	Unitless	Impedance factor
f_C	Unitless	Mass fraction of clay in soil
C_1	W m^{-1} K^{-1}	Parameter to estimate apparent thermal conductivity
C_2	W m^{-1} K^{-1}	Parameter to estimate apparent thermal conductivity
C_3	Unitless	Parameter to estimate apparent thermal conductivity
C_4	W m^{-1} K^{-1}	Parameter to estimate apparent thermal conductivity
C_5	Unitless	Parameter to estimate apparent thermal conductivity
F_1	Unitless	Empirical parameter
F_2	Unitless	Empirical parameter

[20] A site-specific parameterization process is conducted at each site. For tundra sites, measurements at Atqasuk (2001–2008) are used for model calibration in which we modify parameter values (Table 2) to minimize the difference between modeled and measured daily averaged soil temperature at selected depths. Data sets from other tundra sites with similar vegetation cover are used for validation; we use the optimized parameter values from the calibration process to run the simulations. For the two Bonanza Creek forest sites (2003–2008), we use the first 3-year data set for model calibration and the remaining for validation. In addition, the four sites from Hess Creek are used for validation of black spruce sites that varied with stand age and aspect.

3.3. Model Testing

[21] To examine the sensitivity of soil temperature to fire severity, we conduct simulations for two burned sites at Hess Creek (1967 Burn, 2003 Burn) and one unburned site (HCCN). All three sites are located on north-facing slopes. We further use a north- and a south-facing slope at Hess Creek to investigate the influence of aspect on soil temperature at different depths. The sensitivity of soil temperatures to air temperature is assessed by imposing increases of daily surface temperature ranging from $-10°C$ to $10°C$ in $0.01°C$ intervals (∼2000 simulations for each stand). Here, the surface temperature perturbations are imposed as constant anomalies on top of the observed surface temperature.

[22] Furthermore, to evaluate the effect of climate warming on soil temperature profiles, we conduct simulations for all sites using four Intergovernmental Panel on Climate Change (IPCC) emission scenarios, A1FI, A2, B1, and B2 for the period 2001–2100 [*IPCC*, 2007]. These four distinct emission scenarios reflect the implementation of specific policies for controlling anthropogenic greenhouse gases in the future. A1FI corresponds to the largest temperature and precipitation increase. The A2 scenario corresponds to a relatively fast rate of temperature and precipitation increase,

but not as large as that in A1FI. In contrast, the B1 scenario corresponds to a much smaller temperature and precipitation increase than A2. B2 represents a world where the rate of warming is lower than the A2 scenario but higher than B1. Among these four scenarios, A1FI and B1 respectively represent the largest and lowest fossil fuel emissions and atmospheric CO_2 concentrations. In this study, the monthly climate data series are converted into daily series based on the method presented in *Zhuang et al.* [2004].

4. Results

4.1. Model Calibration and Validation

[23] We calibrate the model for tundra sites using temperature and moisture profiles at Atqasuk (2001–2008; Figure 2). The modeled daily soil temperatures agree well with the observed daily values. Calibrated model parameters are then applied to other tundra sites (e.g., West Dock high, 2004–2008; Figure 3), where we also observe good agreement between modeled and observed soil temperatures. The modeled soil temperatures are comparable to observations throughout the entire soil profile (e.g., West Dock high, Figure 4). However, the discrepancy between modeled and measured soil temperatures increases with profile depth. For example, the root mean square error (RMSE) from comparison between modeled and measured soil temperatures generally increases from the top to bottom soil layers (Tables 3a and 3b). The largest error occurs at the Toolik tundra site, and the soil temperature RMSE is clearly larger than those at the other sites. We attribute it to the poor simulation of soil moistures and the more complex soil properties at this site. In addition to the variability associated with depth, the model performance also shows seasonal characteristics in soil thermal dynamics (e.g., Figure 4). During spring, the snowmelt infiltrates into near-surface soil horizons and then re-freezes, creating a period when temperatures hover around 0°C. In fall, temperatures persist at 0°C due to the effects of latent heat exchange during phase change, commonly referred to as the "zero-degree curtain." Based on our simulations, these zero-degree temperatures at seasonal boundaries (spring thaw and autumn freezeup), could persist for several days or weeks in spring and in fall time. Generally, these seasonal boundaries last longer in the boreal forest stands than in the tundra stands.

[24] Our model appears to underestimate soil temperatures during the spring thaw period and fall freezeup and overestimate soil temperatures during summer. In particular, our model overpredicts soil temperatures above the freezing point, and underpredicts soil temperatures from the freezing point down to a threshold that depends on soil depth. A possible reason is that in spring thawing period, our model underestimates the conductivities within the top layers, thereby leading to a lower correlation between soil temperature in top layers and the surface temperature. During fall freezing period, our model tends to underestimate the latent heat exchange within the ice/water transition process. Consequently, this results in a faster freezing period in the top layer soils. In summer time, an overestimation of soil moisture is responsible to the over-predicted soil temperatures. Nevertheless, the model performs well in simulating winter soil temperatures.
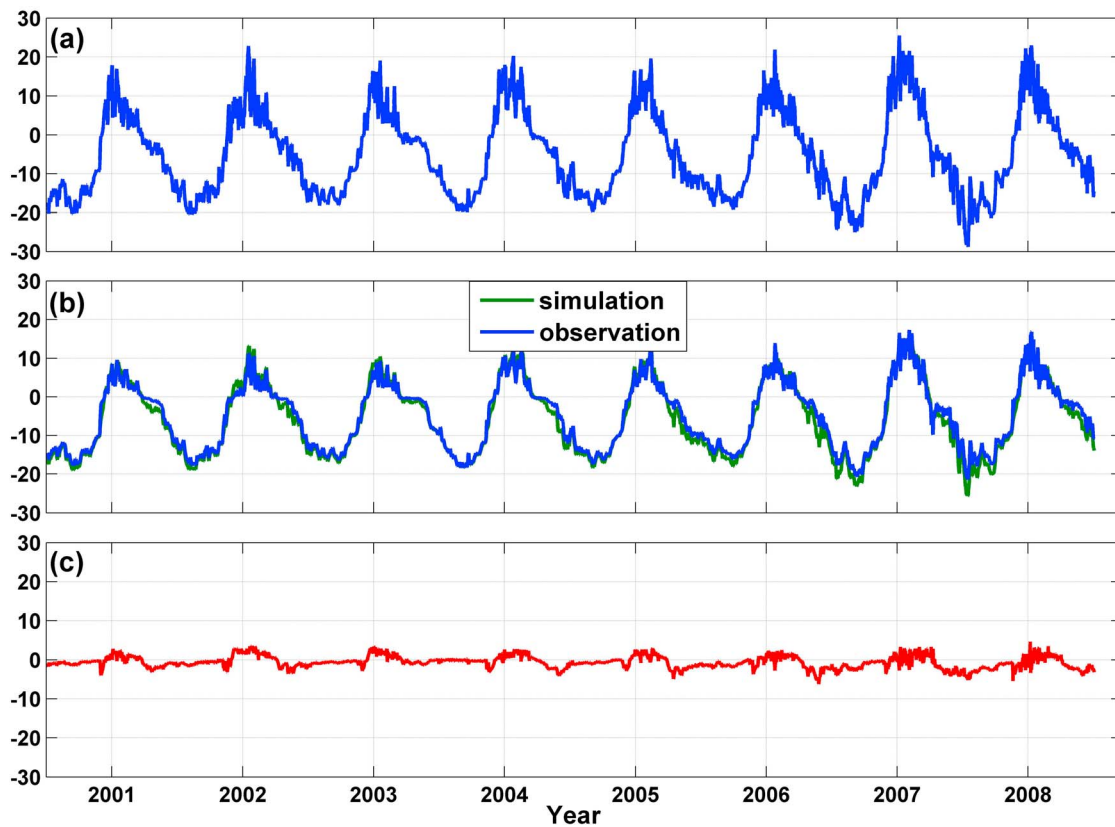
Figure 2. (a) Measurements of surface temperature (°C), (b) modeled soil temperature (°C) at 10 cm depth, and (c) divergence (°C) between modeled and measured 10 cm depth soil temperature at the Atqasuk site.

4.2. Comparing Soil Thermal Dynamics in White and Black Spruce Stands

[25] For boreal forest sites, modeled soil temperatures agree well with measurements for BNZ-B in Bonanza Creek (Figure 5). Similar to tundra sites, the model has a better performance for upper layers than for lower layers. Comparisons of modeled results against measurements show reasonable RMSE values for all studied sites (Tables 3a and 3b). Generally, the model tends to overestimate soil temperatures in the upper layers while underestimating soil temperatures in the lower layers.

[26] Based on results from the ensemble simulations, we obtain the soil-to-surface temperature ratio, which is calculated as the slope of a linear regression of the magnitude of annual variations in modeled soil temperature at depth against the magnitude of annual variations in surface temperature. The derived ratios show that the magnitude of changes in soil temperatures in response to the change in surface temperature decreases as the depth increases. In the very bottom layer, the changing value is always constant since the heat flux is significantly small. At depths from 0 to 3 m, the soil temperature at BNZ-B seems to be more sensitive to the surface temperature than that at BNZ-W in that the same surface temperature increase could lead to higher increase in soil temperatures at BNZ-B (Figure 6). This could be attributed to the difference in soil thermal properties between these two sites. In this case, the black spruce stand has permafrost and is wetter than the white spruce stand. As a result, the effective thermal conductivity is higher in the

black spruce stand, and soil temperature responds more rapidly to fluctuations in surface temperature.

4.3. Modeling Soil Temperature for Burned Black Spruce Stands

[27] The model performs well in simulating soil temperature for burned sites, such as the 2003 burn site in Hess Creek (Figure 7). The modeled soil temperature profile shows only a small difference from measured values when the soil profile is frozen in winter. In summer, the model slightly overestimates the soil temperature, especially for the upper layers. As shown in Figure 6, soil temperatures in the more recently burned stand (HC03) are more sensitive to the surface temperature change, compared with those in the older burned stand (HC67). This indicates that fire increases ALT and the soil thaws immediately following fire, but in this instance, as the ecosystem recovers (i.e., re-growth of organic horizon), the permafrost also recovers.

[28] Compared with unburned sites (e.g., the north-facing slope in Hess Creek, HCCN), results for burned stands (HC67 and HC03) reveal that fires could strengthen the correlation between soil temperatures in lower layers and the surface temperature (Figure 6). It is partly because fires reduce organic-soil horizon thickness, and in turn, increase the thermal conductivity of near-surface soils. Consequently, soil temperatures in burned stands are more sensitive to fluctuations in surface temperature than they are in unburned stands. This implies that fires have the potential to accelerate thawing processes at near-surface layers in permafrost regions,
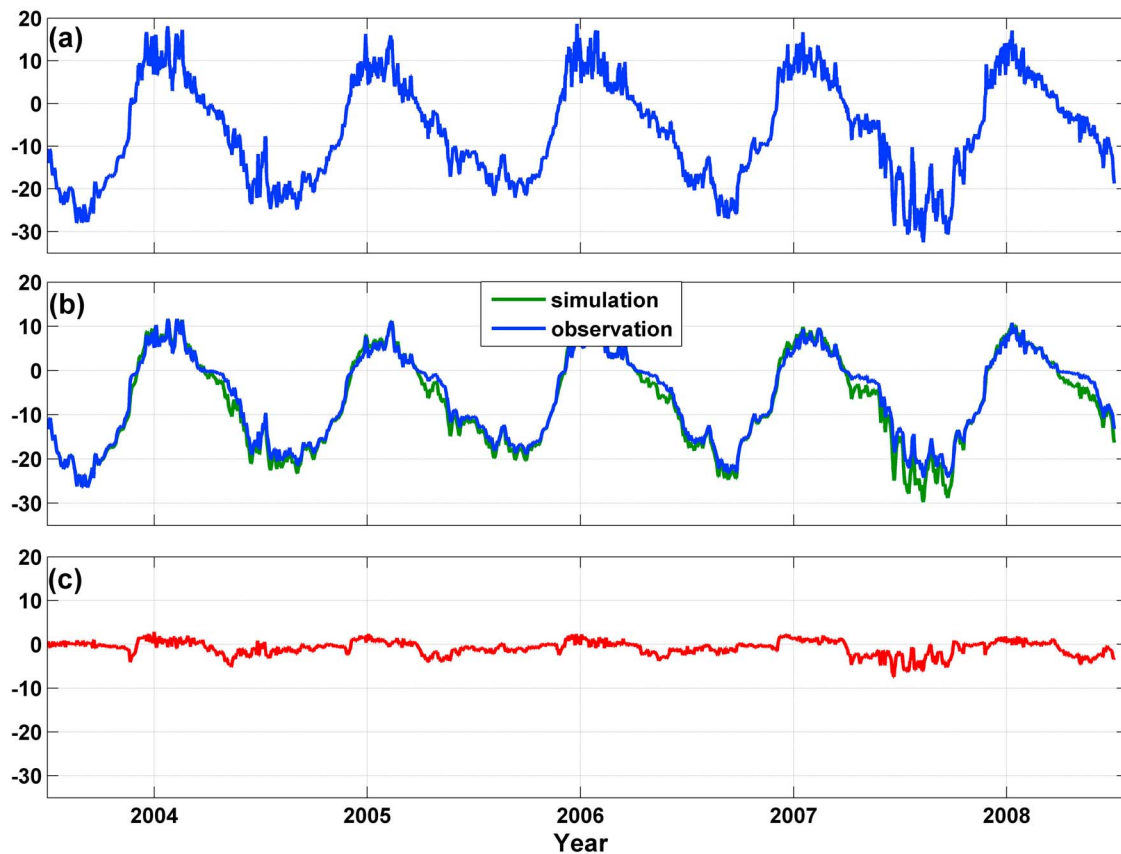
Figure 3. (a) Measurements of surface temperature (°C), (b) modeled soil temperature (°C) at 10 cm depth, and (c) divergence (°C) between modeled and measured 10 cm depth soil temperature at the Westdock high site (using probe 1 data).

which is consistent with findings from previous studies [e.g., *Yoshikawa et al.*, 2003; *O'Donnell et al.*, 2011a, 2011b].

4.4. Modeling Soil Temperature as a Function of Aspect

[29] For upland black spruce forests on both north- and south-facing slopes, our model performs well in simulating soil temperatures at different depths (Table 3b). The south-facing forest stand (HCCS) generally has a warmer surface temperature and a warmer soil temperature and consequently ALT in HCCS is deeper than that in HCCN. In addition, it seems that soil temperatures at the south-facing slope are more sensitive to surface temperature change (Figure 6).

[30] Based on the 2,000 simulations with different surface temperature perturbations, we found that HCCN would reach an equilibrium condition in terms of the correlation with surface temperature at a shallower depth (approximately 50 cm, Figure 6). In contrast, it would be at much greater depth for HCCS to reach the stationary condition (deeper than 3 m). Furthermore, the surface temperature has a stronger influence on soil temperatures through all depths at HCCS relative to the HCCN stand.

4.5. Projection of Soil Temperature Change for 2010–2100

[31] Driven by four IPCC scenarios, our simulations predict an increase in ALT as the air temperature warms in the coming decades (Figure 8). This is not surprising because soil temperatures at different depths are all positively correlated with the surface temperature, which is governed by air temperature [*Yi et al.*, 2009]. Among the four scenarios, A1FI and B1 always correspond to the largest and smallest increase of ALT, respectively.

[32] Under the same climate, different stands exhibit distinct ALT changes in terms of rate and magnitude. In particular, burned stands (i.e., HC67 and HC03) are more sensitive to warming air temperatures relative to unburned stands (i.e., HCCN), in terms of the ALT change (Figure 8). The two burned stands show similar ALT increases in the current century; however, the more recently burned stand (HC03) has a slightly larger ALT increase. Here, we should note that because the model does not take into account changes in OHT following fire, some uncertainty in projected ALT changes remains, especially for the burned stands.

[33] An interesting finding is that the Atqasuk tundra site shows much faster and larger ALT increases than the Toolik site and even a historically much warmer black spruce stand (i.e., HCCN). The major reason is that the projected surface temperatures (i.e., upper boundary conditions) from IPCC in the Atqasuk stand are always higher those in the Toolik stand from October to March, therefore lengthening the thawing period in the Atqasuk stand. Another interesting finding is that the Toolik stand has a similar ALT-changing
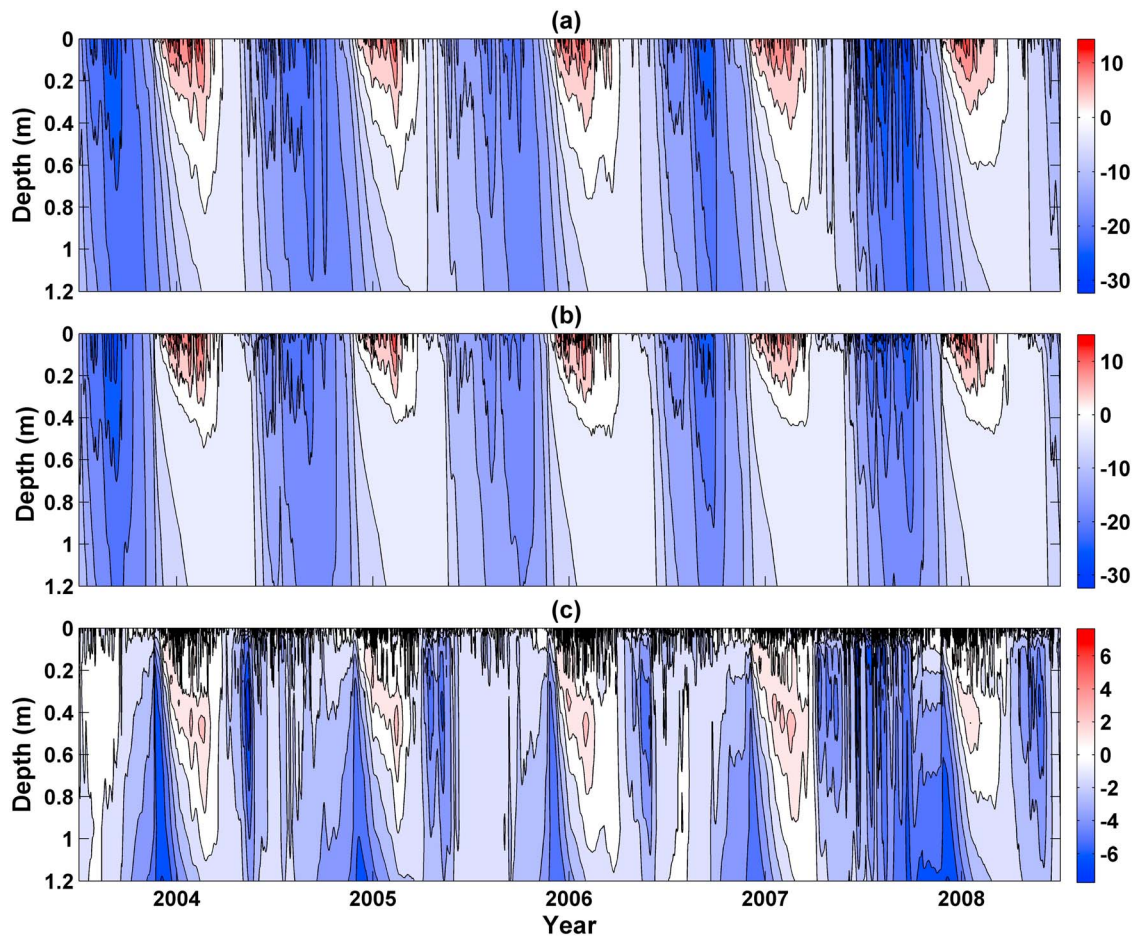
Figure 4. (a) Modeled soil temperatures (°C), (b) measured soil temperatures (°C), and (c) residuals (°C) between the modeled and measured soil temperatures for the West Dock high site (using probe 1 data).

trend to that of the Hess Creek stand (i.e., HCCN) which is a much warmer stand. The reason is that the upper soil layers in HCCN are much less conductive than those in the Toolik stands, and therefore the rate of heat transport from surface to soil is much slower in the HCCN stand, even though the surface temperature is much higher than that in the Toolik stand.

[34] Regardless of differences in soil properties between the north- and south-facing slopes in Hess Creek, ALTs of both slopes exhibit continuous upward trends as air temperature warms. Generally, HCCS shows a much faster rate and higher magnitude of increase (Figure 9). In the first half century, the ALT in HCCS could reach a depth of more than 2 m with an initial value of about 80 cm in 2010, while the ALT in HCCN remains almost consistent at about 50 cm. Both estimations in 2100 are comparable to the measurements taken in 2007, which show a 79 cm ALT at HCCS and a 45 cm ALT at HCCN. In the second half of the 21st century, the ALT increase in the HCCN stand would be much faster under the A1FI and A2 scenarios.

5. Discussion

5.1. Soil Thermal Dynamics at Sites Underlain by Permafrost

[35] Permafrost is an integral component of northern high-latitude ecosystems and plays an important role in regulating the vegetation distribution, soil carbon, and water budgets [*Tchebakova et al.*, 2009; *Yi et al.*, 2009; *Tarnocai et al.*, 2009]. To model permafrost dynamics and evaluate the consequent ecological influence, it is important to account for phase changes with explicit consideration of freezing and thawing processes. The model applied in this study uses an algorithm presented in *Hansson et al.* [2004] to simulate the seasonal variations in soil temperatures and interannual variability in ALT from the present to the year 2100 in permafrost regions. The results indicate that the model performs well in reproducing the soil temperature profile at the site level.

[36] Our results reveal that the major error of the modeled soil temperatures occurs in the summer period when near-surface soil horizons of the active layer are thawed. One possible reason is that the model cannot adequately track rapid changes in soil moisture in the upper layers during summer. By contrast, the model does an excellent job of simulating winter soil temperature, perhaps due to the reduced variability in winter soil moisture. Furthermore, the presence of snow cover during winter acts as a low-conductivity layer, thus buffering soil temperatures against cold extremes in winter [*Nowinski et al.*, 2010; *O'Donnell et al.*, 2011a]. Another reason for this seasonal difference in model performance is that during summer, the unfrozen soil of the active layer enhances interaction of water and soil within the newly

Table 3a. The Root Mean Square Error Values by Comparisons of the Model Simulations Against in Situ Measurements for Atqasuk, Betty Pingo, Sagwon, Toolik, West Dock High Sites, the White Spruce Stand and the Black Spruce Stand in Bonanza Creek

Depth	Atqasuk	Betty Pingo1	Betty Pingo2	Sagwon	Toolik	Westdock high1	Westdock high2	Westdock high3	Westdock high4	BNZ-W[a]	BNZ-B[b]
5 cm	1.04	0.93	1.17	1.19		1.14	1.16	0.90	1.14	3.52	1.91
10 cm	1.38	1.09	1.28	1.86	2.77	1.47	1.57	1.13	1.57	3.54	1.99
15 cm	1.95	1.21	1.59	2.43	4.38	1.60	1.90	1.47	1.96		
20 cm	2.22	1.22	1.65	2.56		1.59	2.03	1.57	2.07	3.21	1.63
25 cm	2.27	1.27	1.69	2.58	4.82	1.75	2.19	1.68	2.18		
30 cm	2.35	1.31	1.85	2.57	4.67	1.80	2.30	1.76	2.25		
35 cm	2.49					1.92	2.45	1.80	2.32		
40 cm		1.37	1.93	2.61	4.84						
45 cm	2.53				5.08	2.04	2.52	1.75	2.34		
50 cm		1.44	1.97	2.57						2.62	1.15
60 cm		1.52	1.99	2.51	5.51						
70 cm	2.21	1.53	1.98	2.45		1.98	2.74	1.59	2.27		
80 cm		1.61	2.06	2.45	5.68						
95 cm	2.29	1.70	2.15	2.44		2.07	2.98	1.55	2.32		
100 cm					5.89					1.50	0.56
120 cm	2.33	1.89	2.29	2.62		2.42	3.33	1.80	2.59		
200 cm										1.68	0.44

[a]BNZ-B: black spruce stand at Bonanza Creek.
[b]BNZ-W: white spruce stand at Bonanza Creek.

thawing portion of the near-surface soil horizons, consequently enabling a complex variety of biogeochemical processes prevented by the frozen soil in winter time [*Khvorostyanov et al.*, 2008]. This increases the uncertainty and variability in modeling the temperature in the newly thawed soil. For these reasons and also due to the relatively moderate fluctuation of surface temperature and water flow in winter, the model performs more successfully in modeling winter soil temperatures. Future efforts could incorporate this soil thermal model into a well-developed ecosystem model (e.g., TEM [*Zhuang et al.*, 2001, 2002, 2003; *Yi et al.*, 2009]), which is able to provide reasonable surface-water and energy budgets.

[37] Historically, ALT in boreal forest sites could be deeper (>2 m) than that in tundra sites (<1 m; compare Figure 5 and Figure 4) due to the difference of climate and soil properties. In our simulations, the warmer air temperature with more conductive soils in boreal forest stands lead to larger ALT compared with the tundra stands. The second reason boreal forest sites might have greater ALT is that the climates at tundra sites are colder than those in boreal forest sites. In addition, the thickness and period of snow cover is larger and longer in tundra sites, shortening the summer thaw period. Since permafrost in the boreal forest is closer to thaw at 0°C, it is more vulnerable to warming conditions [*Osterkamp et al.*, 2000]. However, a more recent synthesis of permafrost temperature trends [*Romanovsky et al.*, 2010] shows that rates of warming have slowed as permafrost temperatures approach 0°C, presumably due to latent heat effects. Further efforts are needed to explore the effect of latent heat transport on the thermal state of permafrost.

[38] The buffering effect of the low-conductivity surface organic-soil layers on soil temperatures in deep layers is profound for both tundra and boreal forest sites, especially during summer. Therefore, compared with that in lower layers, soil temperature in deeper layers is less responsive to the fluctuation of surface temperature. Consequently, a reduction in amplitude and a time-lag remain in soil temperature seasonality with depth. Furthermore, a mild winter

temperature exerts a strong effect on ALT by preventing energy loss from underlying soil in winter, which is consistent with findings in *Wania et al.* [2009].

5.2. Fire Impact on Soil Thermal Dynamics

[39] Fires have a direct prompt effect on soil thermal properties since fire may burn off the surface plant canopy and a great proportion of the surface organic-soil layer, consequently resulting in an instantaneous increase in soil temperature [*Swanson*, 1996; *Burn*, 1998]. Similar to *O'Donnell et al.* [2011a], our model simulates higher volumetric water content and consequently, higher thermal conductivity in HC03, compared with HC67. One possible reason for the higher soil water content is that the fires reduce rates of evapotranspiration and interception as shown in *Moody and*

Table 3b. The Root Mean Square Error Values by Comparisons of the Model Simulations Against in Situ Measurements for the 1967 and 2003 Burned Stands and a North-Facing and a South-Facing Mature Stand at Hess Creek

Depth	HC67[a]	HC03[b]	HCCN[c]	HCCS[d]
2 cm			1.19	
3 cm	1.01	0.39		0.98
5 cm			2.77	
6 cm	1.48			
8 cm		0.79		
9 cm				1.46
11 cm	2.26			
13 cm		1.23		
16 cm			1.67	
20 cm	1.90			
24 cm				2.07
51 cm			2.42	
60 cm				1.58
74 cm	2.71			
81 cm		0.49		
200 cm			1.75	1.18

[a]HC67: 1967 burned stand at Hess Creek.
[b]HC03: 2003 burned stand at Hess Creek.
[c]HCCN: north-facing mature stand at Hess Creek.
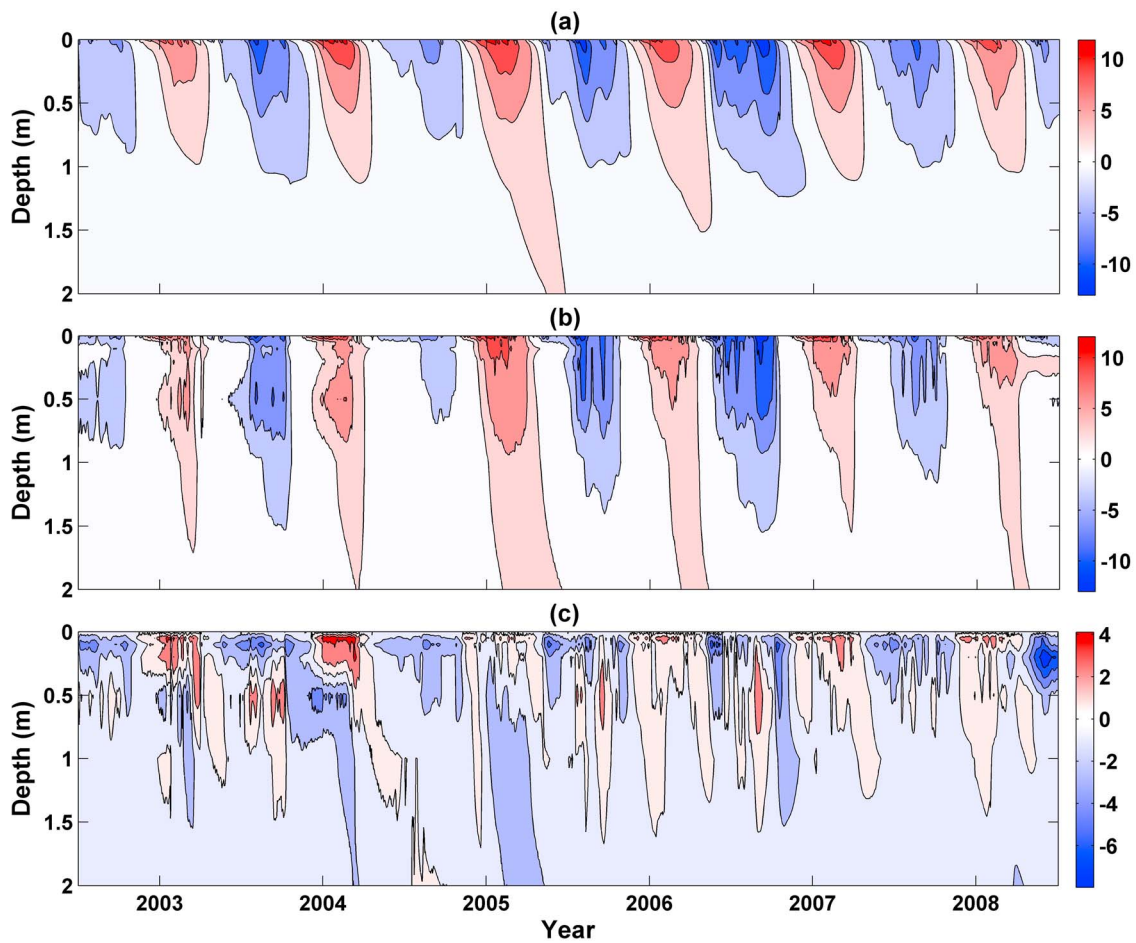[d]HCCS: south-facing mature stand at Hess Creek.

Figure 5. (a) Modeled soil temperatures (°C), (b) measured soil temperatures (°C), and (c) residuals (°C) between the modeled and measured soil temperatures for the Bonanza Creek black spruce site.
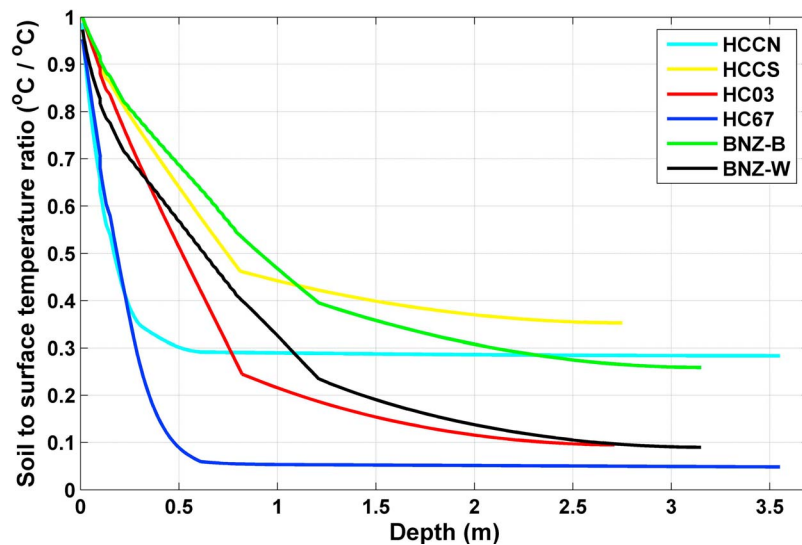

Figure 6. Correlation of soil-to-surface temperature. The value of the ratio is estimated as the slope of a simple linear regression of modeled soil temperature at different depths against surface temperature based on approximately 2000 ensemble simulations for each stand with different upper boundary conditions.

Figure 7. (a) Modeled soil temperatures (°C), (b) measured soil temperatures (°C), and (c) residuals (°C) between the modeled and measured soil temperatures for the 2003 burned site at the Hess Creek black spruce site. It should be noted that this burned site only has four depths of measurement, while the model produced temperatures at 120 separate depths.

Martin [2001]. The moisture-driven increase in thermal conductivity accounts for the observation that soil temperatures in the 2003 site are more correlated to the surface temperature (Figure 6). Consequently, our findings indicate that combustion of surface organic-soil horizons during fire result in high post-fire variability in soil temperature in near-surface layers by increasing the heat conduction which further leads to a thickening in ALT.

[40] Compared with the unburned mature stands in the north-facing slope (HCCN) which has thicker organic horizon, the projected ALT increase is much larger in the two burned stands (i.e., HC67 and HC03) during the 21st century. This is consistent with findings in *O'Donnell et al.* [2011b], who observes a negative exponential relationship between active layer thickness and organic horizon thickness. Wildfire has the potential to decrease the thickness of insulating moss and organic-soil horizons and thus facilitate heat transport from surface to deep soil layers. This implies that the climate-driven increases in permafrost thaw could be exacerbated by fire disturbance during the current century. As climate warms, the interaction of climate and wildfire could first contribute to an increase in ALT and thawing of near-surface permafrost, as findings in previous studies

indicate [e.g., *Hinzman et al.*, 2003; *Johnstone et al.*, 2010]. Future efforts to quantify the effects of wildfire on permafrost should take into account the interaction of organic-soil properties, mineral soil texture, ground ice content, and soil drainage.

5.3. Soil Thermal Regimes in North- and South-Facing Slopes

[41] In interior Alaska north-facing slopes typically have thicker organic-soil horizons and therefore have more thermal insulation than south-facing slopes, and the latter potentially receive more solar insolation. Consequently, soil temperature is generally higher on south-facing slopes than on north-facing slopes. In the present study, the north-facing slope (i.e., HCCN) is drier and thus has lower thermal conductivity values, therefore limiting heat transport from the soil surface to the deep layers.

[42] Soil temperatures at both slopes are sensitive to air temperature and ALT is highly responsive to warming air temperatures, which is consistent with the findings in *Hinkel and Nelson* [2003] and *Demchenko et al.* [2006]. Our projections imply that even under the most modest warming scenario (B1), increases in ALT could be substantial in the
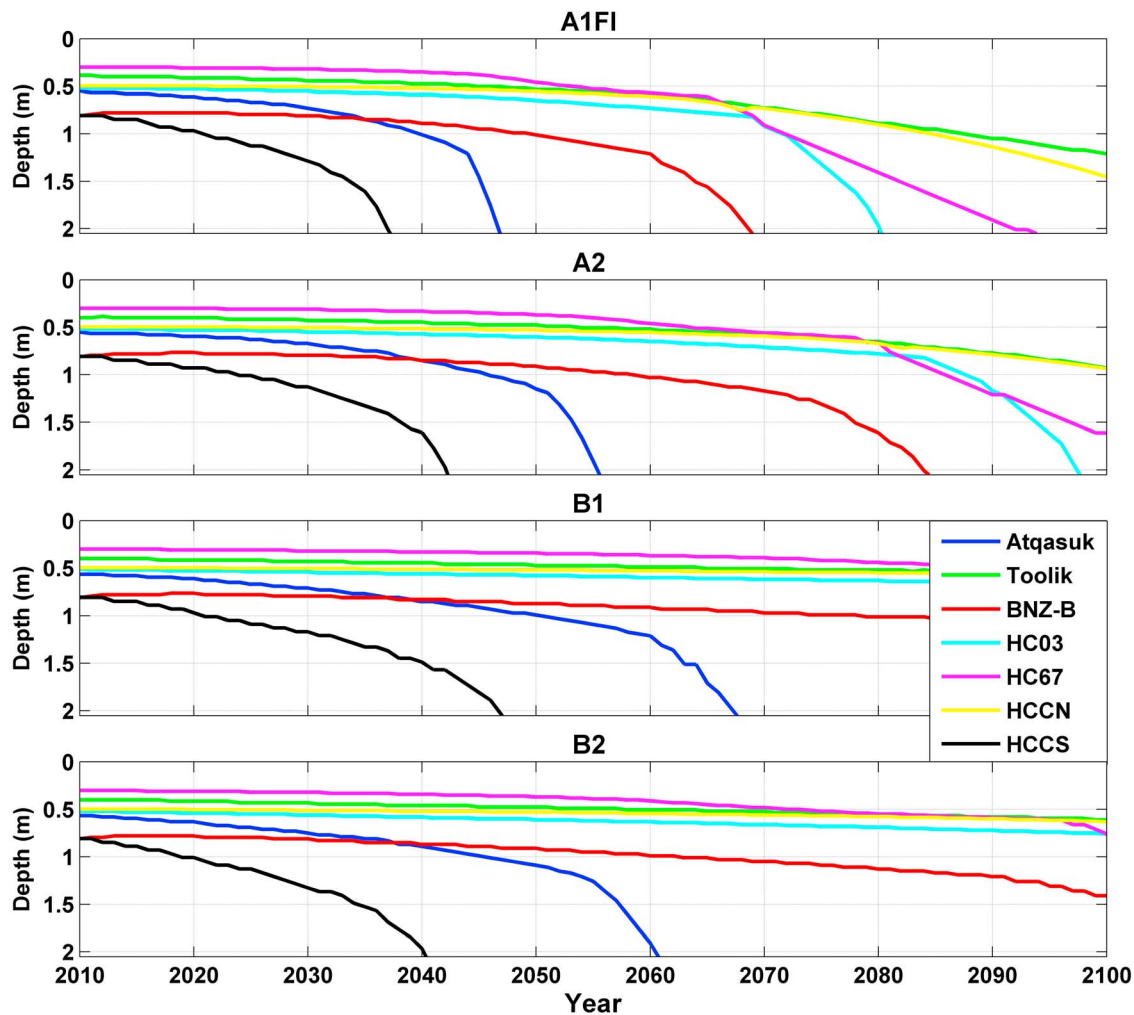
Figure 8. Projected 2010–2100 annual active layer thickness using four IPCC climates scenarios (A1FI, A2, B1 and B2) for Atqasuk, Toolik, the black spruce (BNZ-B) stand in Bonanza Creek, the burn stands in 2003 (HC03) and in 1967 (HC67) at Hess Creek, and north- (HCCN) and south-facing (HCCS) slopes in Hess Creek, Alaska.

coming decades (e.g., HCCS). Under the warmest scenario (A1FI), the permafrost may disappear in many areas during the second half of the 21st century, which is consistent with findings in previous studies [e.g., *Stendel and Christensen*, 2002; *Lawrence et al.*, 2008].

[43] One of the most profound consequences of the projected permafrost thawing is that the carbon balance could be much altered, which further exerts a positive feedback to the climate system [*Koven et al.*, 2011; *Schaefer et al.*, 2011]. In turn, the permafrost thawing could be accelerated by the warming climate due to the positive feedback through the newly released carbon by microbial decomposition of previously frozen organic soil [*Zimov et al.*, 2006a, 2006b; *Schuur et al.*, 2008]. Furthermore, the potential permafrost degradation could have significant impacts on hydrological conditions, biogeochemical processes [e.g., *Nelson*, 2003; *Smith et al.*, 2005], and vegetation change [*Sturm et al.*, 2005]. In addition, the enhanced soil drainage or drier conditions could increase the probability of wildfire occurrence [*Yoshikawa et al.*, 2003]. The continuous thickening of active layers could intensify the potential thermokarst

development which could destroy the surface plants (e.g., spruce and birch forest) and further change the arctic ecological systems [*Osterkamp et al.*, 2000; *Jiang et al.*, 2012].

6. Conclusion

[44] This study applies a recently developed soil thermal model for fully coupled heat transport and water flow for permafrost regions. This model has a distinct advantage over previous models as it provides numerically stable, energy- and mass-conservative solutions. It performs well in simulating soil temperature profiles at both tundra and boreal forest sites. Compared with the tundra ecosystem, the boreal forest ecosystem could be less stable following permafrost degradation. Fires have dramatic and instantaneous effects on active layer thickness change and could potentially lead to an unstable ecosystem in summer. South-facing slopes generally have warmer soil temperatures and much deeper active layer thickness than north-facing slopes. As the climate warms, both tundra and boreal forest stands experience significant permafrost thawing, while the rate and magnitude are
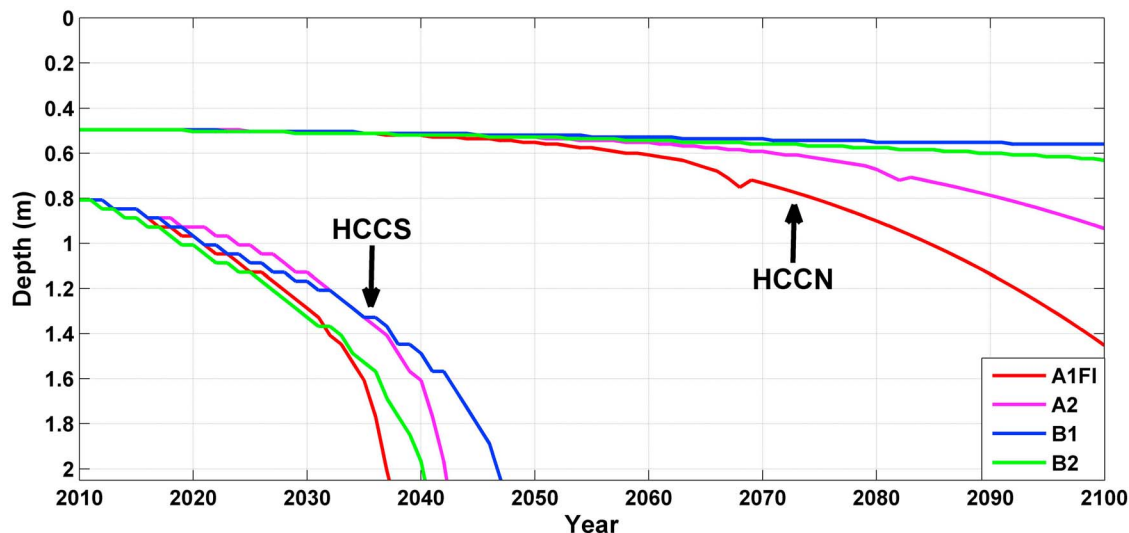
Figure 9. Projected 2010–2100 daily time series of active layer thickness for north-facing (HCCN) and south-facing (HCCS) slopes, using four IPCC climates scenarios (A1FI, A2, B1 and B2).

different and would be influenced by wildfires. Our analysis provides useful tools and information on the investigation of the effect of future climate warming and wildfire disturbance on soil thermal dynamics in permafrost regions. Furthermore, the model presented in this study, which fully couples water and heat transfer, is recommended for incorporation into some ecosystem models (e.g., TEM).

References

Alexeev, V. A., D. J. Nicolsky, V. E. Romanovsky, and D. M. Lawrence (2007), An evaluation of deep soil configurations in the CLM3 for improved representation of permafrost, *Geophys. Res. Lett.*, *34*, L09502, doi:10.1029/2007GL029536.

Amiro, B., A. Orchansky, A. Barr, T. Black, S. Chambers, F. Chapin III, M. Goulden, M. Litvak, H. Liu, and J. McCaughey (2006), The effect of post-fire stand age on the boreal forest energy balance, *Agric. For. Meteorol.*, *140*, 41–50, doi:10.1016/j.agrformet.2006.02.014.

Arctic Climate Impact Assessment (ACIA) (2005), *Arctic Climate Impact Assessment*, Cambridge Univ. Press, New York.

Burn, C. R. (1998), The response (1958–1997) of permafrost and near-surface ground temperatures to forest fire, Takhini River valley, southern Yukon Territory, *Can. J. Earth Sci.*, *35*, 184–199, doi:10.1139/e97-105.

Camill, P. (2005), Permafrost thaw accelerates in boreal peatlands during late-20th century climate warming, *Clim. Change*, *68*, 135–152, doi:10.1007/s10584-005-4785-y.

Demchenko, P. F., A. V. Eliseev, M. M. Arzhanov, and I. I. Mokhov (2006), Impact of global warming rate on permafrost degradation, *Izv. Russ. Acad. Sci. Atmos. Oceanic Phys., Engl. Transl.*, *42*(1), 32–39, 10.1134/S0001433806010026.

Euskirchen, E. S., et al. (2006), Importance of recent shifts in soil thermal dynamics on growing season length, productivity and carbon sequestration in terrestrial high-latitude ecosystems, *Global Change Biol.*, *12*, 731–750, doi:10.1111/j.1365-2486.2006.01113.x.

Fan, Z., J. C. Neff, J. W. Harden, T. Zhang, H. Veldhuis, C. I. Czimczik, G. C. Winston, and J. A. O'Donnell (2011), Water and heat transport in boreal soils: Implications for soil response to climate change, *Sci. Total Environ.*, *409*, 1836–1842, doi:10.1016/j.scitotenv.2011.02.009.

Fayer, M. J. (2000), UNSAT-H Version 3.0: Unsaturated soil water and heat flow model: Theory, user manual, and examples, report, Pac. Northwest Natl. Lab., Richland, Wash.

Goodrich, L. E. (1982), The influence of snow cover on the ground thermal regime, *Can. Geotech. J.*, *24*, 160–163.

Goulden, M. L., et al. (1998), Sensitivity of boreal forest carbon balance to soil thaw, *Science*, *279*, 214–217, doi:10.1126/science.279.5348.214.

Hansson, K., J. Šimůnek, M. Mizoguchi, L. Lundin, and M. T. van Genuchten (2004), Water flow and heat transport in frozen soil: Numerical solution and freeze–thaw applications, *Vadose Zone J.*, *3*, 693–704, doi:10.2113/3.2.693.

Harden, J. W., K. P. O'Neill, S. E. Trumbore, H. Veldhuis, and B. J. Stocks (1997), Moss and soil contributions to the annual net carbon flux of a maturing boreal forest, *J. Geophys. Res.*, *102*, 28,805–28,816, doi:10.1029/97JD02237.

Harden, J., K. L. Manies, M. R. Turetsky, and J. C. Neff (2006), Effects of wildfire and permafrost on soil organic matter and soil climate in interior Alaska, *Global Change Biol.*, *12*, 2391–2403, doi:10.1111/j.1365-2486.2006.01255.x.

Hinkel, K. M., and F. E. Nelson (2003), Spatial and temporal patterns of active layer thickness at Circumpolar Active Layer Monitoring (CALM) sites in northern Alaska, 1995–2000, *J. Geophys. Res.*, *108*(D2), 8168, doi:10.1029/2001JD000927.

Hinzman, L., M. Fukuda, D. V. Sandberg, F. S. Chapin III, and D. Dash (2003), FROSTFIRE: An experimental approach to predicting the climate feedbacks from the changing boreal fire regime, *J. Geophys. Res.*, *108*(D1), 8153, doi:10.1029/2001JD000415.

Iman, R., and J. Helton (1988), An investigation of uncertainty and sensitivity analysis techniques for computer models, *Risk Anal.*, *8*, 71–90, doi:10.1111/j.1539-6924.1988.tb01155.x.

Intergovernmental Panel on Climate Change (IPCC) (2007), *Climate Change 2007: The Physical Science Basis—Contribution of Working Group I to the Fourth Assessment Report of the Intergovernmental Panel on Climate Change*, edited by S. Solomon et al., Cambridge Univ. Press, Cambridge, U. K.

Jiang, Y., Q. Zhuang, S. Schaphoff, S. Sitch, A. Sokolov, D. Kicklighter, and J. Melillo (2012), Uncertainty analysis of vegetation distribution in the northern high latitudes during the 21st century with a dynamic vegetation model, *Ecol. Evol.*, *2*(3), 593–614, doi:10.1002/ece3.85.

Johnstone, J. F., F. S. Chapin III, T. N. Hollingsworth, M. C. Mack, V. Romanovsky, and M. Turetsky (2010), Fire, climate change, and forest resilience in interior Alaska, *Can. J. For. Res.*, *40*, 1302–1312, doi:10.1139/X10-061.

Jorgenson, M. T., and T. E. Osterkamp (2005), Response of boreal ecosystems to varying modes of permafrost degradation in Alaska, *Can. J. For. Res.*, *35*, 2100–2111, doi:10.1139/x05-153.

Jorgenson, M. T., C. H. Racine, J. C. Walters, and T. E. Osterkamp (2001), Permafrost degradation and ecological changes associated with a warming climate in central Alaska, *Clim. Change*, *48*, 551–579, doi:10.1023/A:1005667424292.

Jorgenson, M. T., Y. L. Shur, and E. R. Pullman (2006), Abrupt increase in permafrost degradation in Arctic Alaska, *Geophys. Res. Lett.*, *33*, L02503, doi:10.1029/2005GL024960.

Jorgenson, M. T., V. Romanovsky, J. Harden, Y. Shur, J. O'Donnell, E. A. G. Schuur, M. Kanevskiy, and S. Marchenko (2010), Resilience and vulnerability of permafrost to climate change, *Can. J. For. Res.*, *40*, 1219–1236, doi:10.1139/X10-060.

Kane, E. S., D. W. Valentine, E. A. G. Schuur, and K. Dutta (2005), Soil carbon stabilization along climate and productivity gradients in black spruce forests of interior Alaska, *Can. J. For. Res.*, *35*, 2118–2129, doi:10.1139/x05-093.

Khvorostyanov, D. V., et al. (2008), Vulnerability of permafrost carbon to global warming. Part I: Model description and role of heat generated by organic matter decomposition, *Tellus, Ser. B*, *60*, 250–264, doi:10.1111/j.1600-0889.2007.00333.x.

Koven, C. D., B. Ringeval, P. Friedlingstein, P. Ciais, P. Cadule, D. Khvorostyanov, G. Krinner, and C. Tarnocai (2011), Permafrost carbon-climate feedbacks accelerate global warming, *Proc. Natl. Acad. Sci. U. S. A.*, *108*, 14,769–14,774, doi:10.1073/pnas.1103910108.

Lawrence, D. M., and A. G. Slater (2008), Incorporating organic soil into a global climate model, *Clim. Dyn.*, *30*, 145–160, doi:10.1007/s00382-007-0278-1.

Lawrence, D. M., A. G. Slater, V. E. Romanovsky, and D. J. Nicolsky (2008), Sensitivity of a model projection of near-surface permafrost degradation to soil column depth and representation of soil organic matter, *J. Geophys. Res.*, *113*, F02011, doi:10.1029/2007JF000883.

Lawrence, D. M., A. G. Slater, and S. C. Swenson (2012), Simulation of present-day and future permafrost and seasonally frozen ground conditions in CCSM4, *J. Clim.*, *25*, 2207–2225, doi:10.1175/JCLI-D-11-00334.1.

Marchenko, S., V. E. Romanovsky, and G. Tipenko (2008), Numerical modeling of spatial permafrost dynamics in Alaska, in *Ninth International Conference on Permafrost*, edited by D. L. Kane and K. M. Hinkel, pp. 1125–1130, Inst. of Northern Eng., Univ. of Alaska Fairbanks, Fairbanks.

Moody, J. A., and D. A. Martin (2001), Post-fire rainfall intensity-peak discharge relations for three mountainous watersheds in the western USA, *Hydrol. Processes*, *15*, 2981–2993, doi:10.1002/hyp.386.

Nelson, F. E. (2003), (Un)frozen in time, *Science*, *299*, 1673–1675, doi:10.1126/science.1081111.

Noborio, K., K. J. McInnes, and J. L. Heilman (1996), Two-dimensional model for water, heat and solute transport in furrow-irrigated soil: I. Theory, *Soil Sci. Soc. Am. J.*, *60*, 1001–1009, doi:10.2136/sssaj1996.03615995006000040007x.

Nowinski, N. S., L. Taneva, S. E. Trumbore, and J. M. Welker (2010), Decomposition of old organic matter as a result of deeper active layers in a snow depth manipulation experiment, *Oecologia*, *163*, 785–792, doi:10.1007/s00442-009-1556-x.

O'Donnell, J. A., M. R. Turetsky, J. W. Harden, K. L. Manies, L. E. Pruett, G. Shetler, and J. C. Neff (2009), Interactive effects of fire, soil climate, and moss on CO_2 fluxes in black spruce ecosystems of interior Alaska, *Ecosystems*, *12*, 57–72, doi:10.1007/s10021-008-9206-4.

O'Donnell, J. A., J. W. Harden, A. D. McGuire, and V. E. Romanovsky (2011a), Exploring the sensitivity of soil carbon dynamics to climate change, fire disturbance and permafrost thaw in a black spruce ecosystem, *Biogeosciences*, *8*, 1367–1382, doi:10.5194/bg-8-1367-2011.

O'Donnell, J. A., J. W. Harden, A. D. McGuire, M. Z. Kanevskiy, M. T. Jorgenson, and X. M. Xu (2011b), The effect of fire and permafrost interactions on soil carbon accumulation in an upland black spruce ecosystem of interior Alaska: Implications for post-thaw carbon loss, *Global Change Biol.*, *17*, 1461–1474, doi:10.1111/j.1365-2486.2010.02358.x.

Osterkamp, T. E. (2007), Characteristics of the recent warming of permafrost in Alaska, *J. Geophys. Res.*, *112*, F02S02, doi:10.1029/2006JF000578.

Osterkamp, T. E., L. Viereck, Y. Shur, M. T. Jorgenson, C. Racine, L. Falcon, A. Doyle, and R. D. Boone (2000), Observations of Thermokarst and its impact on boreal forests in Alaska, U.S.A, *Arct. Antarct. Alp. Res.*, *32*, 303–315.

Pavlov, A. V. (1994), Current changes of climate and permafrost in the arctic and sub-arctic of Russia, *Permafrost Periglacial Processes*, *5*, 101–110, doi:10.1002/ppp.3430050204.

Payette, S., A. Delwaide, M. Caccianiga, and M. Beauchemin (2004), Accelerated thawing of subarctic peatland permafrost over the last 50 years, *Geophys. Res. Lett.*, *31*, L18208, doi:10.1029/2004GL020358.

Randerson, J. T., et al. (2006), The impact of boreal forest fire on climate warming, *Science*, *314*, 1130–1132, doi:10.1126/science.1132075.

Romanovsky, V. E., S. L. Smith, and H. H. Christiansen (2010), Permafrost thermal state in the polar northern hemisphere during the International Polar Year 2007–2009: A synthesis, *Permafrost Periglacial Processes*, *21*, 106–116, doi:10.1002/ppp.689.

Saito, H., J. Šimůnek, and B. P. Mohanty (2006), Numerical analysis of coupled water, vapor, and heat transport in the vadose zone, *Vadose Zone J.*, *5*, 784–800, doi:10.2136/vzj2006.0007.

Sazonova, T. S., V. E. Romanovsky, J. E. Walsh, and D. O. Sergueev (2004), Permafrost dynamics in the 20th and 21st centuries along the East Siberian transect, *J. Geophys. Res.*, *109*, D01108, doi:10.1029/2003JD003680.

Schaefer, K., T. Zhang, L. Bruhwiler, and A. P. Barrett (2011), Amount and timing of permafrost carbon release in response to climate warming, *Tellus, Ser. B*, *63*, 165–180, doi:10.1111/j.1600-0889.2011.00527.x.

Schneider von Deimling, T., M. Meinshausen, A. Levermann, V. Huber, K. Frieler, D. M. Lawrence, and V. Brovkin (2012), Estimating the near-surface permafrost-carbon feedback on global warming, *Biogeosciences*, *9*, 649–665, doi:10.5194/bg-9-649-2012.

Schuur, E. A. G., et al. (2008), Vulnerability of permafrost carbon to climate change: Implications for the global carbon cycle, *BioScience*, *58*(8), 701–714, doi:10.1641/B580807.

Schuur, E. A. G., J. G. Vogel, K. G. Crummer, H. Lee, J. O. Sickman, and T. E. Osterkamp (2009), The effect of permafrost thaw on old carbon release and net carbon exchange from tundra, *Nature*, *459*, 556–559, doi:10.1038/nature08031.

Serreze, M. C., J. E. Walsh, F. S. Chapin III, T. Osterkamp, M. Dyurgerov, V. Romanovsky, W. C. Oechel, J. Morison, T. Zhang, and R. G. Barry (2000), Observational evidence of recent change in the northern high-latitude environment, *Clim. Change*, *46*, 159–207, doi:10.1023/A:1005504031923.

Smith, L. C., Y. Sheng, G. M. MacDonald, and L. D. Hinzman (2005), Disappearing arctic lakes, *Science*, *308*, 1429, doi:10.1126/science.1108142.

Soja, A., N. Tchebakova, N. French, M. Flannigan, H. Shugart, B. Stocks, A. Sukhinin, E. Parfenova, F. Chapin III, and P. Stackhouse (2007), Climate-induced boreal forest change: Predictions versus current observations, *Global Planet. Change*, *56*, 274–296, doi:10.1016/j.gloplacha.2006.07.028.

Stendel, M., and J. H. Christensen (2002), Impact of global warming on permafrost conditions in a coupled GCM, *Geophys. Res. Lett.*, *29*(13), 1632, doi:10.1029/2001GL014345.

Stieglitz, M., S. J. Dery, V. E. Romanovsky, and T. E. Osterkamp (2003), The role of snow cover in the warming of arctic permafrost, *Geophys. Res. Lett.*, *30*(13), 1721, doi:10.1029/2003GL017337.

Sturm, M., T. Douglas, C. Racine, and G. E. Liston (2005), Changing snow and shrub conditions affect albedo with global implications, *J. Geophys. Res.*, *110*, G01004, doi:10.1029/2005JG000013.

Swanson, D. K. (1996), Susceptibility of permafrost soils to deep thaw after forest fires in interior Alaska, U.S.A., and some ecological implications, *Arct. Alp. Res.*, *28*, 217–227, doi:10.2307/1551763.

Tang, J., and Q. Zhuang (2010), Modeling soil thermal and hydrological dynamics and changes of growing season in Alaskan terrestrial ecosystems, *Clim. Change*, *107*, 481–510, doi:10.1007/s10584-010-9988-1.

Tarnocai, C., J. G. Canadell, E. A. G. Schuur, P. Kuhry, G. Mazhitova, and S. Zimov (2009), Soil organic carbon pools in the northern circumpolar permafrost region, *Global Biogeochem. Cycles*, *23*, GB2023, doi:10.1029/2008GB003327.

Tchebakova, N., E. Parfenova, and A. Soja (2009), The effects of climate, permafrost and fire on vegetation change in Siberia in a changing climate, *Environ. Res. Lett.*, *4*, 045013, doi:10.1088/1748-9326/4/4/045013.

Wania, R., I. Ross, and I. C. Prentice (2009), Integrating peatlands and permafrost into a dynamic global vegetation model: 1. Evaluation and sensitivity of physical land surface processes, *Global Biogeochem. Cycles*, *23*, GB3014, doi:10.1029/2008GB003412.

Werdin-Pfisterer, N. R., K. Kielland, and R. D. Boone (2009), Soil amino acid composition across a boreal forest successional sequence, *Soil Biol. Biochem.*, *41*, 1210–1220, doi:10.1016/j.soilbio.2009.03.001.

Wisser, D., S. Marchenko, J. Talbot, C. Treat, and S. Frolking (2011), Soil temperature response to 21st century global warming: The role of and some implications for peat carbon in thawing permafrost soils in North America, *Earth Syst. Dyn.*, *2*, 121–138, doi:10.5194/esd-2-121-2011.

Yi, S., et al. (2009), Interactions between soil thermal and hydrological dynamics in the response of Alaska ecosystems to fire disturbance, *J. Geophys. Res.*, *114*, G02015, doi:10.1029/2008JG000841.

Yoshikawa, K., W. R. Bolton, V. E. Romanovsky, M. Fukuda, and L. D. Hinzman (2003), Impacts of wildfire on the permafrost in the boreal forests of interior Alaska, *J. Geophys. Res.*, *108*, 8148, doi:10.1029/2001JD000438. [printed *108*(D1), 2003].

Zhuang, Q., V. E. Romanovsky, and A. D. McGuire (2001), Incorporation of a permafrost model into a large-scale ecosystem model: Evaluation

of temporal and spatial scaling issues in simulating soil thermal dynamics, *J. Geophys. Res.*, *106*(D24), 33,649–33,670, doi:10.1029/2001JD900151.

Zhuang, Q., A. D. McGuire, K. P. O'Neill, J. W. Harden, V. E. Romanovsky, and J. Yarie (2002), Modeling the soil thermal and carbon dynamics of a fire chronosequence in Interior Alaska, *J. Geophys. Res.*, *107*, 8147, doi:10.1029/2001JD001244. [printed *108*(D1), 2003].

Zhuang, Q., et al. (2003), Carbon cycling in extratropical terrestrial ecosystems of the Northern Hemisphere during the 20th Century: A modeling analysis of the influences of soil thermal dynamics, *Tellus, Ser. B*, *55*, 751–776, doi:10.1034/j.1600-0889.2003.00060.x.

Zhuang, Q., J. M. Melillo, D. W. Kicklighter, R. G. Prinn, D. A. McGuire, P. A. Steudler, B. S. Felzer, and S. Hu (2004), Methane fluxes between terrestrial ecosystems and the atmosphere at northern high latitudes during the past century: A retrospective analysis with a process-based biogeochemistry model, *Global Biogeochem. Cycles*, *18*, GB3010, doi:10.1029/2004GB002239.

Zimov, S. A., E. A. G. Schuur, and F. S. Chapin III (2006a), Permafrost and the global carbon budget, *Science*, *312*, 1612–1613, doi:10.1126/science.1128908.

Zimov, S. A., S. P. Davydov, G. M. Zimova, A. I. Davydova, E. A. G. Schuur, K. Dutta, and F. S. Chapin III (2006b), Permafrost carbon: Stock and decomposability of a globally significant carbon pool, *Geophys. Res. Lett.*, *33*, L20502, doi:10.1029/2006GL027484.